Numerical Heat Transfer, Part A, 44: 375–397, 2003

ISSN: 1040-7782 print/1521-0634 online
DOI: 10.1080/10407780390210251

Taylor & Francis
Taylor & Francis Group

STEADY NATURAL CONVECTION IN A TILTED LONG CYLINDRICAL ENVELOPE WITH LATERAL ADIABATIC SURFACE, PART 1: THEORETICAL MODELING AND NUMERICAL TREATMENTS

Y. L. He and W. Q. Tao
Xi'an Jiaotong University, Xi'an, China

T. S. Zhao
Hong Kong University of Science and Technology, Kowloon, Hong Kong, China

Z. Q. Chen
Xi'an Jiaotong University, Xi'an, China

The steady natural-convection heat transfer in a tilted cylindrical envelope with constant but different end temperatures (300 and 80 K) is investigated numerically with the lateral surface being adiabatic. The inner diameter of the envelope is 27.8 mm and its length/diameter ratio is 9. This is supposed to be a simplified model for the pulse tube in a pulse-tube cryocooler when the pulse tube is positioned at different orientations. The problem studied is a typical nonlinear one in that the thermophysical properties of the working fluid (helium) vary significant from the hot end to the cold end. Three-dimensional steady-state governing equations are solved with fully variable thermal properties. The high nonlinearity of the problem leads to many special characters of the convergence process, and a very peculiar convergence process is found. Initial-field dependence is also revealed. After quite a few preliminary computations, a series of convergence criteria are proposed. Grid-independence examination is conducted for inclination angle of 110°. It is found that the grid system of $20(r) \times 20(\varphi) \times 80(Z)$ with grids in the z direction being nonuniformly positioned can obtain a grid-independent solution. Preliminary computations are conducted for the horizontal position with 70°C of end temperature difference. The predicted velocity and temperature distributions are compared with available measured data. Good agreement between the predicted and measured results provides strong support for the physical model and numerical treatments developed in this article.

Received 15 July 2002; accepted 25 November 2002.

This work was supported by the National Key Project of Fundamental R&D of China (Grant 2000026303) and the National Natural Science Foundation of China (no. 50276046). The support of these foundations is gratefully acknowledged. Thanks also go to Mr. Ding Wen-Jing for providing some additional computational results.

Address correspondence to W. Q. Tao, Xi'an Jiaotong University, School of Energy and Power Engineering Xi'an, Shaanxi 710049, China. E-mail: wqtao@mail.xjtu.edu.cn

NOMENCLATURE

c_p	specific heat at constant pressure	zw(n)	axial interface position
D	diameter	β	volume expansion coefficient
g	gravitational acceleration	Γ	nominal diffusion coefficient
GM	axial flow rate	η	fluid dynamic viscosity
k	thermal conductivity	θ	inclination angle
L	length of the pulse tube	ρ	fluid density
p	pressure	ϕ	general variable
pr	Prandtl number	φ	circumferential coordinate
Q	heat transfer rate		
r	radius		
Re	Reynolds number	**Subscripts**	
S	source term	c	cold
T	temperature	cond	conduction
u, v, w	velocity components	h	hot
z	axial coordinate	m	mean

1. INTRODUCTION

Natural convection in enclosures is a kind of classical problem in numerical heat transfer, and many numerical and analytical studies have been performed [1–14]. However, most of the previous investigations were based on the following conditions. (1) The so-called Boussinesq assumption was adopted, which is valid for limited value of temperature difference between hot and cold surfaces [15]. For example, for air at the room temperature, the maximum temperature difference for adopting this assumption is below 50°C. (2) As far as the geometric shape is concerned, most studies were conducted for rectangular enclosures [4, 6, 8–10] or annuli [1–3, 5, 7, 11, 12]. Very few investigations were conducted for a long cylindrical envelope with an adiabatic lateral wall. The only two references known to the present authors are [13, 14]. In [13], the fluid flow in a horizontal tube with two ends at different temperatures was solved analytically. However, the flow was treated as a forced convection with constant physical properties. The fluid flow in the pipe was assumed to be composed of an upper portion and a lower portion which were considered as identical except in direction. Obviously, such a flow picture cannot represent the flow pattern in a practical tube because of the large temperature difference between the cold and warm ends. In [14] an asymptotic solution was obtained for the velocity and temperature fields in a horizontal tube with warm and cold ends and an adiabatic lateral surface. The Boussinesq assumption was adopted and the asymptotic solution presented for the velocity and temperature field was valid only for the limiting case where the Rayleigh number based on the end-to-end temperature difference approaches zero. It is evident that the velocity and temperature results provided by [14] cannot describe the natural convection in a pulse tube. As far as experimental work is concerned, the only publication related to the present study is that of Kimura and Bejan [16]. They performed an experimental study of the natural convection in a horizontal tube with the two ends at different but constant temperatures. The Rayleigh number based on the tube diameter ranged from 10^8 to 10^9, with the end temperature difference being around 80°C. Kimura and Bejan found that at each cross section normal to the axial direction, the temperature depth

variation along the vertical diameter is almost linear. In addition, in the cross section through the z–r plane, the measured velocity distributions show that the flow consists of two thin jets, one flowing toward the cold end along the top surface and the other flowing in the opposite direction along the bottom. Due to the viscosity–temperature variation in the vertical direction, velocities in the upper (warm) jet are appreciably larger than those in the lower (cold) jet. Although the test temperature difference of [16] is much less than that of the present study, the Rayleigh number range of the two studies is quite close, hence some comparisons will be made later in this article and in the discussion of the companion article [24].

In order to have a better understanding of the peculiar characters of the natural convection in a pulse tube, the working condition of a pulse-tube cryocooler is briefly presented below. A schematic diagram of the pulse-tube cryocooler is presented in Figure 1. The pulse-tube cryocooler is an attractive device of small cooling capacity that is widely used in aerospace engineering and for military purposes because of its inherent advantages such as no moving parts in the cold stage, low manufacturing cost, reduced mechanical vibration, etc. As shown in Figure 1 the pulse tube itself is a long tube with an inner diameter ranging from several millimeters to tens of millimeters; the ratio of its length to its diameter is usually around 10. Its two ends can be regarded as two isothermal surfaces, with room temperature as the hot end and the lowest temperature it can reach as the cold end. To improve the performance of the pulse-tube cryocooler, the pulse tube is usually made of materials with low thermal conductivity. As a first approximation, its outside surface can be regarded as being adiabatic [17]. With present-day pulse-tube refrigerator technology, the cold-end temperature ranges from 80 K to several degrees Kelvin. The pulse tube may be connected with a pressure-wave generator by a long flexible tube with a length of several meters, thereby reducing the interference noise from the compressor and rotary valve to a negligible level. The flexible connectivity between the compressor and the cold end also allows one to change the orientation of the pulse tube, which is an attractive feature for application. The fluid flow in the pulse-tube system is oscillating, with frequency ranging from 2 Hz to tens of hertz. Different orientations of the pulse tube leads to different relative positions of the hot and cold ends, which may cause natural convection in the enclosure when the frequency is low. From a heat transfer point of view, this is a natural convection in a long cylindrical envelope with an adiabatic lateral wall. A tilted cylindrical envelope is described in Figure 2,

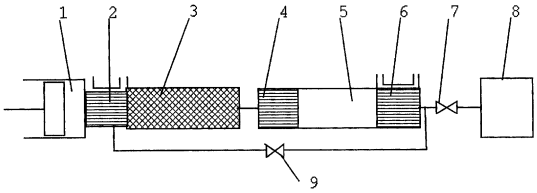

1. Pressure wave generator 2. Water cooler 3. Regenerator 4. Cold end heat exchanger 5. Pulse tube 6. Hot end heat exchanger 7. Orifice valve 8. Reservoir 9. Double inlet valve

Figure 1. Schematic diagram of pulse tube refrigerator.

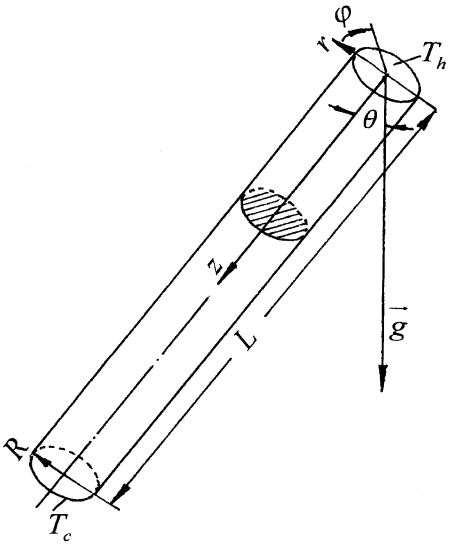

Figure 2. Coordinates and geometry of the cylindrical envelope.

where the origin of the Z coordinate is fixed at the hot end and θ is the angle between the axis of the pulse tube and the direction of gravity. When $\theta = 0$, the hot end is up and the cold end is down; for $\theta = 180$, the situation is the opposite. Thummes et al. [18] reported their experiments in this regard, and found a profound effect of the natural convection in the pulse tube on the cooling capacity of a pulse-tube cryocooler. They also adopted some available heat transfer correlations for the natural convection in cylindrical enclosures at different orientations and estimated the heat transfer rate by these correlations. They obtained the heat transfer rate of the natural convection in the pulse tube from their experimental net cooling power and from the prediction of the correlations. In the θ range from 0 to 70°, and at $\theta = 180°$, they obtained qualitative agreement, while in the range $\theta = 70$–$180°$ the correlations they adopted only roughly describe the observed variation of heat transfer rate. In the present authors' opinion, such an outcome may be expected since the correlations they adopted are all based on small-temperature-difference cases, which cannot take the effect of the severe variation in thermal physical properties into account. As indicated before, the temperature difference between the hot and cold ends may be as large as 220 K or more, the conventional Boussinesq assumption is by no means applicable, and full consideration of the variable thermal properties must be taken into account in the analysis of the natural convection.

The purpose of the present study is to perform three-dimensional numerical simulation for the natural convection of helium in a simplified pulse-tube model: a long cylindrical envelope with an adiabatic lateral surface and two isothermal end walls (Figure 2). The flow in the envelope is assumed to be developed by the gravitational force only, because of the difference in the fluid density. As a first approximation, in the low-frequency region (say, several hertz), the natural-convection and the forced-convection flow are assumed to be additive [18]. Hence, the oscillating flow is neglected. This is a common practice in the heat transfer community in

studying mixed or combined convection. For example, for the combined free and forced convection for external or internal flow, the total Nusselt number is expressed as some summation of the natural (or free) convection and forced convection [19]. In addition, the rationality of this practice is also supported by our numerical results of the heat transfer rate between the hot and cold ends: the predicted variation pattern of the heat transfer rate with inclined angle agrees well with the estimated curve based on the test results in [18]. For the simulation of natural convection, we do not adopt the Boussinesq assumption. According to [20], this is a two-part approximation: (1) it neglects all variable property effects in the governing equations, except for the density in the momentum equations; and (2) it approximates the density difference term with a simplified equations of state,

$$\rho_r - \rho = \rho\beta(t - t_r) \tag{1}$$

where β is the volumetric coefficient of thermal expansion (for an ideal gas, $\beta = 1/T_r$), and t_r is a reference temperature. In our computation, the hot end is set at 300 K and the cold end at 80 K. The temperature difference is as large as 220 K. As indicated above, for air it is generally required that the temperature difference be below 50 K, and according to [21], the temperature difference should be less than 40 K, under which the Boussinesq approximation is valid [21]. Thus the above-mentioned Boussinesq assumption is not acceptable, and the variations of the thermal properties (including density) with temperature in all terms of the governing equations should be taken into account. This was implemented by introducing curve-fitting equations for λ, η, c_p, and Pr in the code based on the data provided in [22], and before every iteration the thermophysical properties were calculated from the available temperature field. The gas density was determined by using the state equation of a perfect gas. The length of the tube is 250 mm, and its inner diameter is taken as 27.8 mm ($L/D = 9.0$). The average pressure in the tube is set at 18 bar, corresponding to the average pressure in a practical pulse tube [23]. The curve-fitting equations for the properties are as follows:

$$\eta = 2.00273 \times 10^{-6} + 9.09908 \times 10^{-8} \times T - 1.912514 \times 10^{-10} \times T^2 + 3.4245 \times 10^{-13} \times T^3 - 1.68578 \times 10^{-16} \times T^4 \tag{2a}$$

$$k = 1.27333 \times 10^{-2} + 8.3313 \times 10^{-4} \times T - 3.1432 \times 10^{-6} \times T^2 + 1.04193 \times 10^{-8} \times T^3 - 1.36503 \times 10^{-11} \times T^4 \tag{2b}$$

$$\mathrm{Pr} = 0.69224 - 1.0539 \times 10^{-3} \times T + 1.33212 \times 10^{-5} \times T^2 - 6.1066 \times 10^{-8} \times T^3 + 9.3986 \times 10^{-11} \times T^4 \tag{2c}$$

Computations were conducted for every 10° increment starting from $\theta = 0°$.

In the following presentation, the three-dimensional governing equations of the physical problem will be presented first, followed by a brief description of the numerical methods, including the discretization scheme of the convection and diffusion term. Details will be provided about the convergence characteristics of the iteration

process, including the dependence of the solution on the initial field assumption. A series of convergence criteria will be presented. Then the grid independence of the numerical solution will be examined. Finally, the results of a preliminary computation and comparison with available test data will be provided. Details of numerical results, including the velocity and temperature distributions, are provided in a companion article [24].

2. GOVERNING EQUATIONS AND NUMERICAL METHODS

The three-dimensional governing equations for fluid flow and heat transfer in a cylindrical envelope with variable thermal properties take the following form:

$$\frac{\partial}{\partial z}(\rho u\phi)+\frac{1}{r}\frac{\partial}{\partial r}(r\rho v\phi)+\frac{1}{r}\frac{\partial}{\partial \varphi}(\rho w\phi)=\frac{\partial}{\partial z}\left(\Gamma\frac{\partial \phi}{\partial z}\right)+\frac{1}{r}\frac{\partial}{\partial r}\left(\Gamma r\frac{\partial \phi}{\partial r}\right)+\frac{1}{r}\frac{\partial}{\partial \varphi}\left(\frac{\Gamma}{r}\frac{\partial \phi}{\partial \varphi}\right)+S \tag{3}$$

where ϕ is the general variable, representing u, v, w and T, Γ is the general diffusion coefficient, and S is the general source term. For u, v, w, $\Gamma=\eta$, while for T, $\Gamma=\eta/\mathrm{Pr}$. For a case with variable thermophysical properties, the general source term takes the following form for different variables:

$$u: \quad S=-\frac{\partial p}{\partial z}+\frac{\partial}{\partial z}\left(\eta\frac{\partial u}{\partial z}\right)+\frac{1}{r}\frac{\partial}{\partial r}\left(r\eta\frac{\partial v}{\partial z}\right)+\frac{1}{r}\frac{\partial}{\partial \varphi}\left(\eta\frac{\partial w}{\partial z}\right)+\rho g\cos\theta \tag{4a}$$

$$v: \quad S=-\frac{\partial p}{\partial r}+\frac{\partial}{\partial z}\left(\eta\frac{\partial u}{\partial r}\right)+\frac{1}{r}\frac{\partial}{\partial r}\left(r\eta\frac{\partial v}{\partial r}\right)+\frac{1}{r}\frac{\partial}{\partial \varphi}\left[\eta\frac{r\partial(w/r)}{\partial r}\right]$$
$$-\frac{2\eta}{r}\left(\frac{1}{r}\frac{\partial w}{\partial \varphi}+\frac{v}{r}\right)+\frac{\rho w^2}{r}-\rho g\sin\theta\cos\varphi \tag{4b}$$

$$w: \quad S=-\frac{1}{r}\frac{\partial p}{\partial \varphi}+\frac{\partial}{\partial z}\left(\eta\frac{\partial u}{r\partial \varphi}\right)+\frac{1}{r}\frac{\partial}{\partial r}\left[r\eta\left(\frac{1}{r}\frac{\partial v}{\partial \phi}-\frac{w}{r}\right)\right]$$
$$+\frac{1}{r}\frac{\partial}{\partial \varphi}\left[\eta\left(\frac{1}{r}\frac{\partial w}{\partial \varphi}+\frac{2v}{r}\right)\right]+\frac{\eta}{r}\left[r\frac{\partial(w/r)}{\partial \varphi}+\frac{1}{r}\frac{\partial v}{\partial \varphi}\right]$$
$$-\frac{\rho vw}{r}+\rho g\sin\theta\sin\varphi \tag{4c}$$

It can be seen from Eq. (4) that, apart from the pressure gradient term and the gravitational term, numerous terms of second derivatives of velocities exist, making the discretization and computational procedure very complicated. Actually, Eq. (4*a*) may be rewritten as

$$u: \quad S=-\frac{\partial p}{\partial z}+\eta\frac{\partial^2 u}{\partial z^2}+\frac{\partial u}{\partial z}\frac{\partial \eta}{\partial z}+\eta\frac{1}{r}\frac{\partial}{\partial r}\left(r\frac{\partial v}{\partial z}\right)+\frac{1}{r}\left(r\frac{\partial v}{\partial z}\right)\frac{\partial \eta}{\partial r}$$
$$+\eta\frac{1}{r}\frac{\partial^2 w}{\partial z^2}+\frac{1}{r}\frac{\partial w}{\partial z}\frac{\partial \eta}{\partial \varphi}+\rho g\cos\theta \tag{5}$$

We now adopt an assumption here to simplify the computation: the values of $\partial\eta/\partial z, \partial\eta/\partial r,$ and $\partial\eta/\partial\varphi$ are small, and the terms including them can be neglected. Then, using the mass conservation law expressed by

$$\frac{\partial u}{\partial z} + \frac{1}{r}\frac{\partial}{\partial r}(rv) + \frac{1}{r}\frac{\partial w}{\partial \varphi} = 0 \tag{6}$$

the source terms for the three components of velocity may be simplified as follows:

$$u: \qquad S = -\frac{\partial p}{\partial z} + \rho g \cos\theta \tag{7a}$$

$$v: \qquad S = -\frac{\partial p}{\partial r} + \frac{\rho w^2}{r} - \frac{2\eta}{r^2}\frac{\partial u}{\partial \varphi} - \frac{\eta v}{r^2} - \rho g \sin\theta \cos\varphi \tag{7b}$$

$$w: \qquad S = -\frac{1}{r}\frac{\partial p}{\partial \varphi} - \frac{\rho w v}{r} + \frac{2\eta}{r^2}\frac{\partial v}{\partial \varphi} - \frac{\eta w}{r^2} + \rho g \sin\theta \sin\varphi \tag{7c}$$

The boundary conditions are as follows. For u, v, w: at all solid walls, $u = v = w = 0$; at $\theta = 0$ and $\theta = \pi, u = 0, \partial v/\partial\theta = \partial w/\partial\theta = 0$. For T: $T = T_h$ at $z = 0$; $T = T_c$ at $z = L$; at $r = R, \partial T/\partial r = 0$; at $\theta = 0$ and $\theta = \pi, \partial T/\partial\theta = 0$.

In the above governing equations, the following features are worth noting. First, the gravitational term is presented in the N–S equation as a source term, and it is the only driving source that causes the fluid motion. Since we treat only the natural convection in this article, the boundary conditions at $z = 0$ and $z = L$ for the forced oscillating flow are not included. These two ends are regarded as two solid walls with constant but different temperatures. Second, as indicated above, in the natural convection the driving source of fluid motion is gravity acting on the temperature-dependent density of the fluid. From this point of view the fluid is compressible. However, the compressibility terms in the momentum and energy equations are usually insignificant for the natural convection in an enclosure [21], and hence it is a common practice that the mass conservation equation for incompressible flow is adopted [25]. Third, the dependent variable in the governing energy equation is the fluid temperature, and the corresponding general diffusion coefficient $\Gamma = k/c_p = \eta/\mathrm{Pr}$. From this point of view, the fluid specific heat is taken as constant. However, the variation of specific heat of helium with temperature is not so severe as thermal conductivity or viscosity. In addition, in our computations the variation of Prandtl number with temperature is taken into account, thus largely compensating the above approximation.

The governing equations are discretized by the finite-volume method [26, 27]. The segregated solution algorithm, SIMPLEC, is adopted, where the momentum equations are solved one by one, the pressure field is updated from the mass conservation equation, and the pressure correction is used to revise both the velocity components and pressure. The energy equation is coupled with the momentum equation via the source term, hence is solved simultaneously with the momentum equations. The diffusion and convection terms are discretized by the power-law scheme [26, 27]; the reasons for this choice will be presented later. The resulting

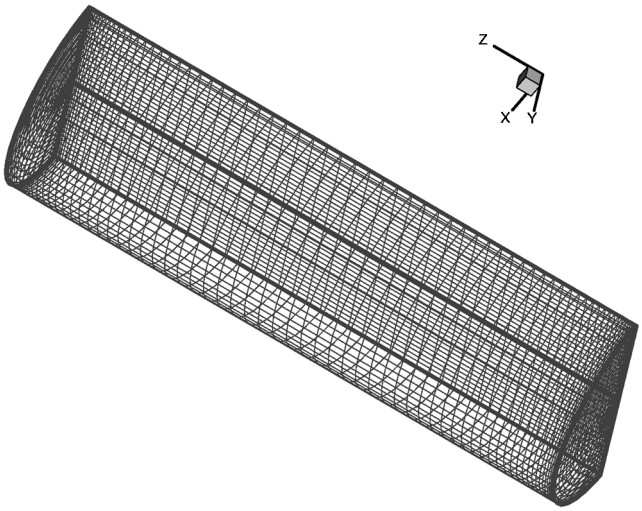

Figure 3. Grid system used in computation.

algebraic equations are solved by the successive line underrelaxation method. The grids are distributed uniformly in the radius and circumferential directions, while nonuniform distribution is adopted in the axial direction, with more grids clustered near the two end walls. The control-volume interface position in the z direction is determined according to the following equation:

$$zw(n) = \left[n/N - \frac{\sin(2\pi n/N)}{2\pi} \right] L \tag{8}$$

where n is the serial number of the interface ($n = 0$ to N) and N is the total number of control volumes in the z direction.

The temperature gradients at the hot and cold walls are determined by a three-point second-order-accurate discretized equation. The two-point formally first-order discretization formulation is also used. Comparison showed that the numerical difference between these two discretized expressions is very small, never larger than 1%. The grid number in three directions is $20(r) \times 20(\varphi) \times 80(z)$. The three-dimensional grid adopted in the computations is shown in Figure 3. To guarantee the convergence of iteration, the relaxation factors for velocity components and temperature were all taken as 0.01.

3. REPRESENTATION OF SOME SPECIAL FEATURES OF THE ITERATIVE PROCEDURE

3.1. Variation Pattern of the Average Axial Flow Rate

The problem at hand is a highly nonlinear one in that the thermophysical properties vary significantly along the axial direction. In Table 1 the values of thermal conductivity et al. at 300 and 80 K are listed [23]. It can be seen that within the envelope the thermal physical properties vary from 2.35 (thermal conductivity) to

Table 1. Thermolphysical properties of helium

Property	300 K	80 K
Thermal conductivity, W/m K	1.505×10^{-1}	6.404×10^{-1}
Dynamic viscosity, kg/m s	1.987×10^{-5}	8.200×10^{-6}
Density, kg/m^3	2.888	1.083×10^{1}
Prandtl number	0.6874	0.6658

3.75 times (density). This makes the convergence of the iterative procedure very difficult. After quite a few preliminary computations with different iteration numbers, it was found that axial flow rate of the fluid is an important index to judge whether the convergence can be regarded as being reached or not. The average axial flow rate is defined as follows:

$$\mathrm{GM} = \frac{1}{N}\sum_{k=1}^{N} \int_{\Omega_k} \rho(i, j, k)\, \mathrm{abs}[w(i,j,k)] r\, dr\, d\varphi \tag{9}$$

where N is the number of sections in the axial direction (77 in total). It should be noted here that the absolute values of the axial velocity $w(i, j, k)$ were used in the above integration. This is because in the control-volume approach the total mass conservation for the flow in an enclosure can be satisfied at a very early stage of iteration, thus if the algebraic values of $w(i, j, k)$were used in the integration, we would get near-zero results in the early stages of iteration. Only by using the absolute value does the integration gradually approach a constant when the iterative process converges. Other characteristic parameters, such as $\rho_{\mathrm{ave}}[\beta L g(T_h - T_c)]^{1/2}$ (which has the physical meaning of buoyancy force for unit volume fluid) is not sensitive to the convergence situation, since all the included quantities are almost fixed during the iteration. It was revealed by our numerical practice that the proposed parameter GM is very sensitive to the iteration convergence. For any orientation of the envelope, the value of GM first increases with iteration, reaches a maximum, and then decreases and gradually approaches constant. The curve of GM versus iteration number ITER for $\theta =$ 100–180° with every 20° is presented in Figure 4. As can be seen there, beyond the summit of the GM–ITER curve, for every inclination there is a short period, ranging from hundreds to thousands of iterations, where GM remains almost constant. However, beyond that region, if iteration is continued, the value of GM gradually changes because of the high nonlinearity of the problem. And up to 40,000 iterations, no trend can be found that the value of GM is approaching constant. If the transport process is of diffusion type, then this value will not change after a certain number of iterations. The curves for $\theta = 0$–80° are presented in Figure 5, where such characteristic variation can be clearly observed. Thus our first convergence criterion is that the value of GM should be in the relatively constant region beyond the summit of the GM–ITER curve for each inclination of the pulse tube.

3.2. Initial Field Dependency of the Numerical Solution

The solutions of highly nonlinear problems may be dependent on the initial fields. That is the case here. A converged solution of the section averaged fluid

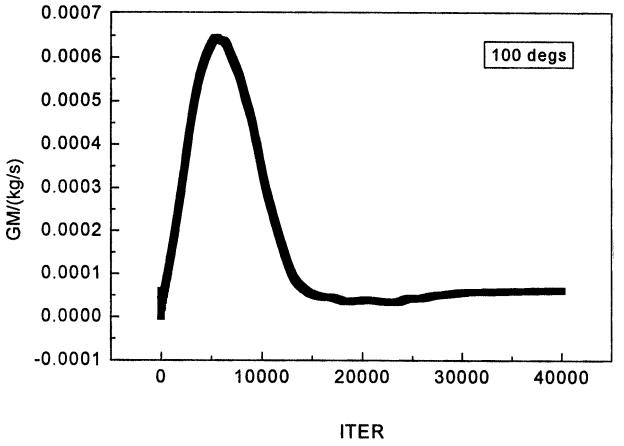

(a) $\theta = 100^\circ$

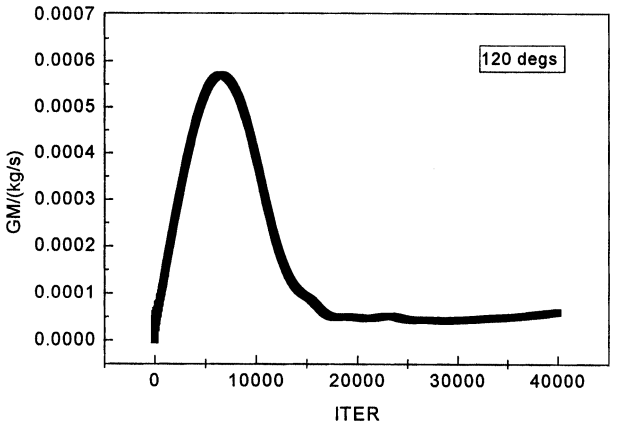

(b) $\theta = 120^\circ$

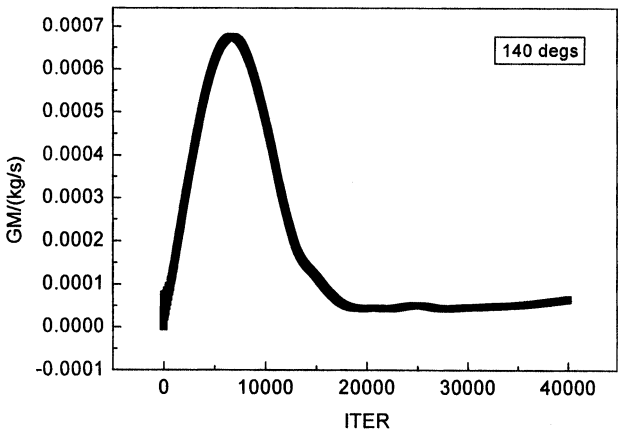

(c) $\theta = 140^\circ$

Figure 4. GM versus iteration number for $\theta = 100$–180°.

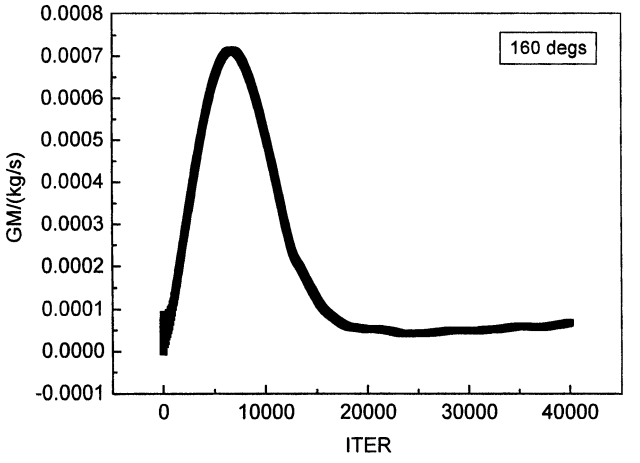

(d) $\theta = 160^\circ$

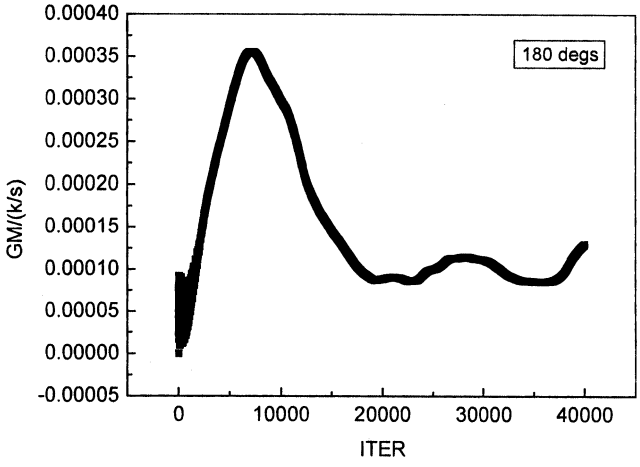

(e) $\theta = 180^\circ$

Figure 4. Continued.

temperature for tilted angle $\theta = 120^\circ$ is shown in Figure 6, where very steep temperature gradients at the cold wall can be observed. For the case of $\theta = 120^\circ$, the hot wall is cooler than the cold wall, hence some natural convection occurs in the envelope. And Figure 6 is a typical axial distribution of a convection-dominated situation. This solution was obtained under a linear distribution for the initial temperature field. Such a temperature variation pattern once was assumed as an initial temperature field for the case of inclination angle 70°, in which the dominant transport mechanism is diffusion. The resulting converged solution gives the temperature distribution shown in Figure 7, which is very much like the one for the convection-dominated situation. However, if we adopt a linear distribution of the axial temperature for $\theta = 70^\circ$, the resulting converged solution for the section average temperature is as presented in Figure 8.

The heat transfer rates between the hot and cold ends of the two solutions were also very different. The one from a linear initial distribution was 0.3067 W, while

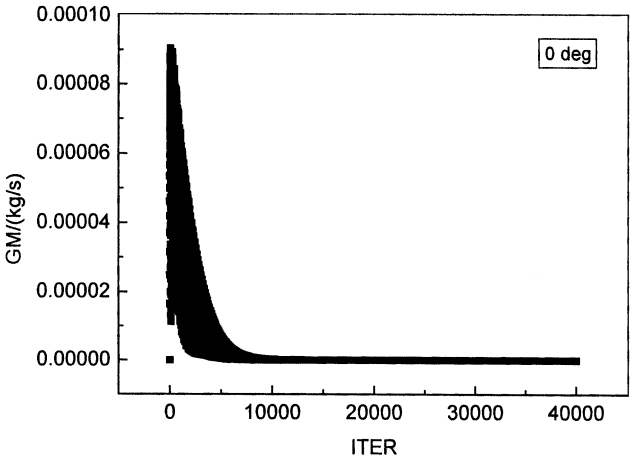

(a) $\theta = 0^\circ$

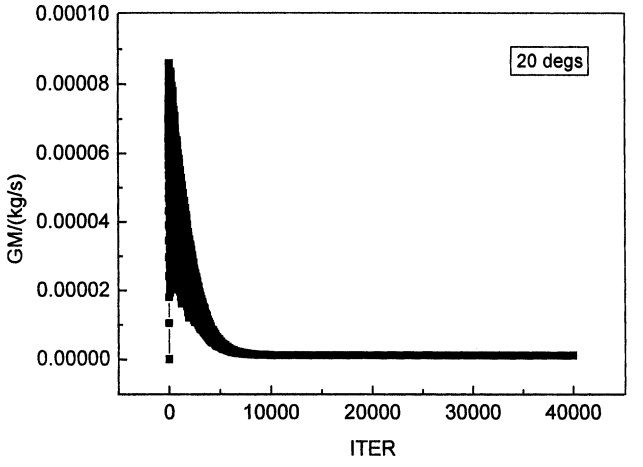

(b) $\theta = 20^\circ$

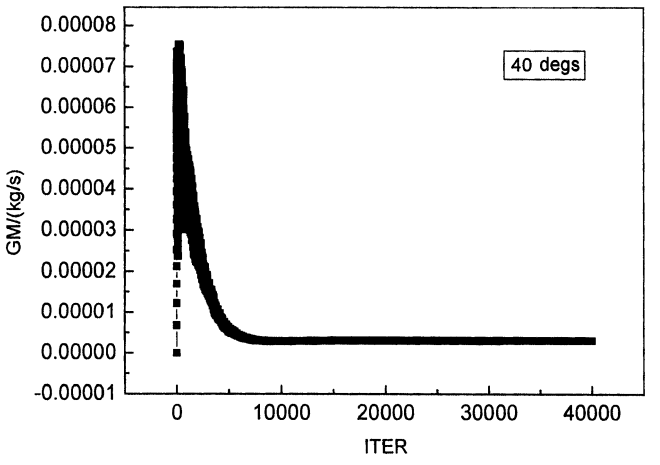

(c) $\theta = 40^\circ$

Figure 5. GM versus iteration number for $\theta = 0$–80°.

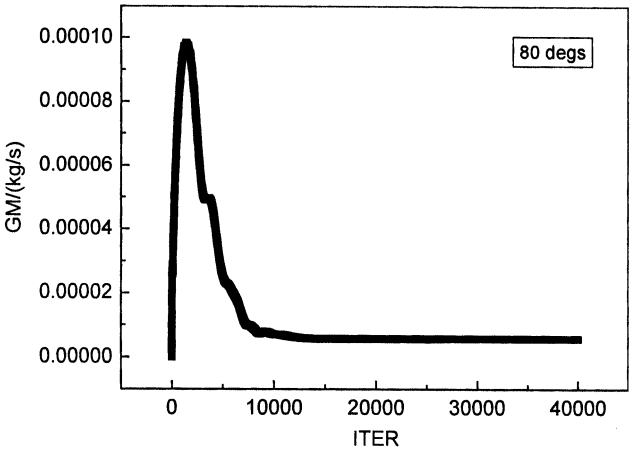

(d) $\theta = 60^\circ$

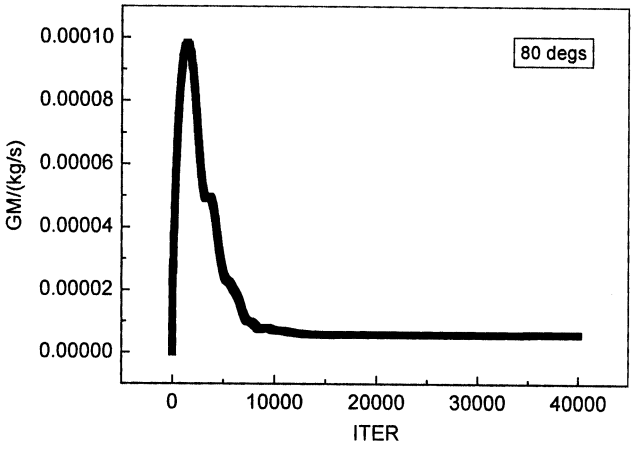

(e) $\theta = 80^\circ$

Figure 5. Continued.

that from an initial field similar to the converged solution of 120° was as large as 5.15 W. It is obvious that the solution with a linear distribution is more reliable and practical. Thus the solutions presented in this article and the companion one were all obtained with a linear distribution of initial temperature. Multiple solutions of nonlinear problems are often seen in the literature [31, 32]. For the cases studied, we would not expect the solution with Z-type initial distribution to be manifested experimentally, since the heat transfer rate is physically unrealistic.

3.3. Discussion of the Discretization Scheme

As indicated before, the power-law scheme was used in the computation. Because the power-law scheme is often treated as a low-order discretization scheme [28], a rationale should be provided to argue for such a choice. Taking the inclination angle of 120° as an example, it is found that when the section average flow rate reaches its maximum, in about 12% of the control volumes the local grid Peclet

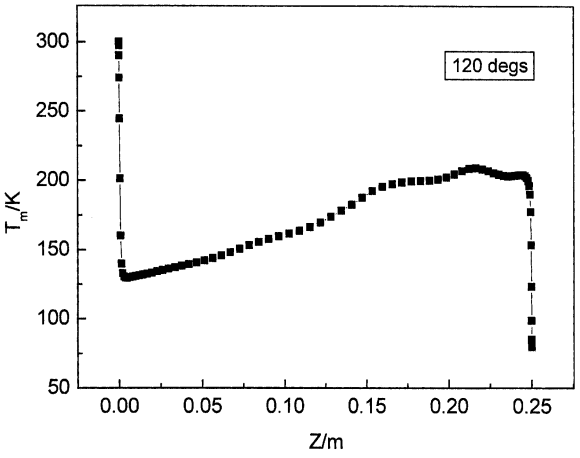

Figure 6. Section averaged axial fluid temperature for $\theta = 120°$ with a linear initial distribution.

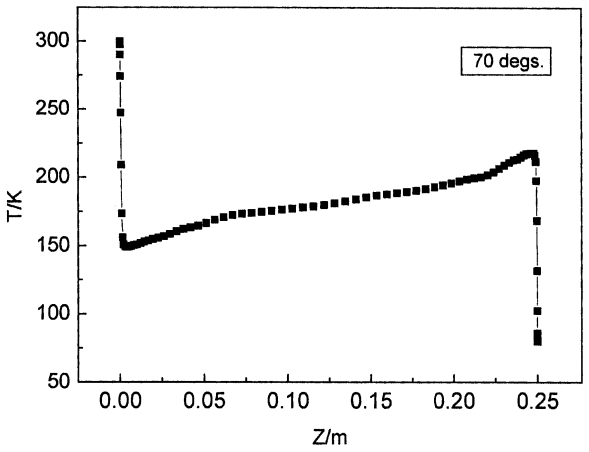

Figure 7. Section averaged axial fluid temperature for $\theta = 70°$ with a Z-type initial distribution.

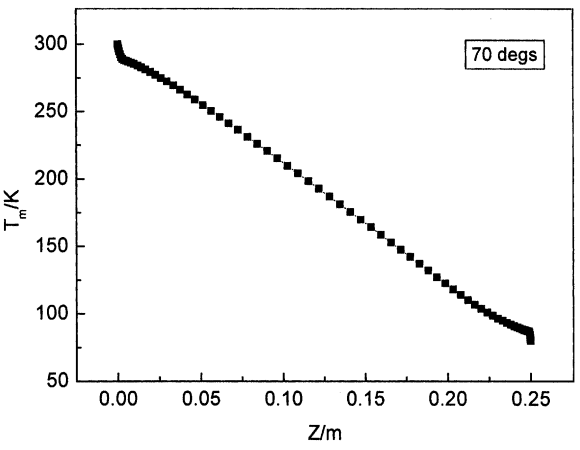

Figure 8. Section averaged axial fluid temperature for titled angle $\theta = 70°$ with a linear initial distribution.

number is larger than 140, with the maximum value being about 2,080. Thus, if we use a conditionally stable scheme, such as central difference or QUICK, oscillation will occur and lead finally to divergence of the solution procedure. The absolutely stable character of the power-law scheme attracted the present authors to adopt it for discretization. The heat transfer rate of the converged solution using the power-law scheme is 7.221 W. To show the rationale for adopting this scheme, we also tested such a combination: before the cross-section averaged flow rate reaches a relatively constant region, the power-law scheme was used, and once this region was reached the scheme was switched to central difference. The final converged solutions for the total heat transfer rate were then compared. The total heat transfer of the combination procedure is 7.144 W, having about 1.07% relative difference compared to the solution of the power-law scheme. Since this difference is trivial, the computational results from the power-law scheme were considered acceptable. It is interesting to point out further that even in the relatively constant and low-flow-rate region there is still 0.8% of the control volumes in which the local grid Peclet number is larger than 140, with the maximum value being about 720. Our numerical simulation showed that under such conditions the central difference for the convection scheme can lead to a nonoscillating solution. This once again shows that the traditional analysis method for the stability of a convection discretization scheme, such as the sign reservation rule proposed in [29], is applicable only qualitatively for practical complex problems, and the actual critical grid Peclet number of the conditionally stable scheme is problem-dependent [30].

4. CONVERGENCE CRITERIA

Based on many preliminary computations, the following conditions were found to be suitable for the judging of iterative convergence.

The first condition is the approaching of a relatively constant value of GM beyond the summit of the GM–ITER curve.

The second criterion is about the relative change of the mean heat transfer rate at the hot and cold ends. It is required that between two successive iterations the relative change of the mean heat transfer rate should be less than 10^{-4}. The variation of the relative thermal balance between the heat transfer rates at the hot and cold ends for $\theta = 60^\circ$ and $\theta = 100^\circ$ is presented in Figure 9. It can be seen there that only after the value of GM is beyond the summit of the GM–ITER curve can the relative change of the average heat transfer rate in the envelope be less than a certain desired small value.

Two more criteria are set up for mass conservation:

$$\text{SMAX/GM} \leq 1. \times 10^{-4} \tag{10a}$$

$$\text{Abs(SSUM/GM)} \leq 1. \times 10^{-6} \tag{10b}$$

where SMAX is the maximum absolute value of the control-volume mass residual, while SSUM is the mass residual of the whole computation domain. Examples of the variations of SMAX/GM and SSUM/GM with iteration number are shown in Figures 10 and 11, for $\theta = 120^\circ$ and $\theta = 180^\circ$, respectively.

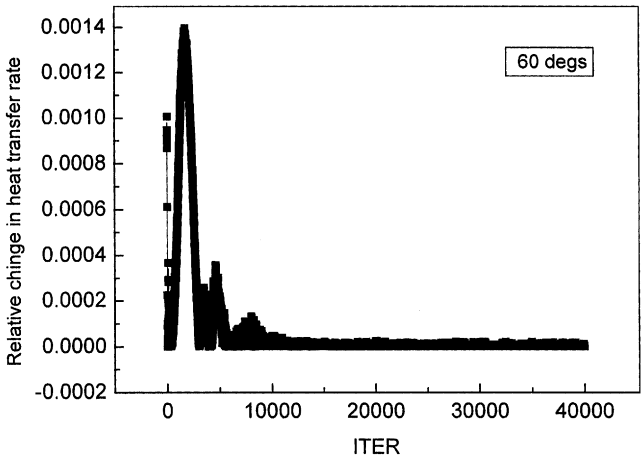

(a) $\theta = 60^{\circ}$

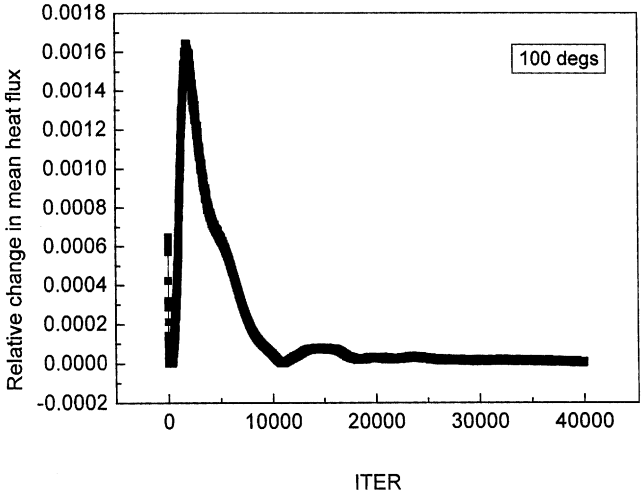

(b) $\theta = 100^{\circ}$

Figure 9. Relative change in average heat transfer rate in the envelope.

The variation of the relative thermal balance, defined as abs$[(Q_h - Q_c)/Q_h]$, with the iteration is presented in Figure 12 for the above two inclination angles. Such a variation pattern is representative for all inclinations. Again we see that the outline of the relative thermal balance variation is more or less similar to that of the GM. Only after the GM passes its summits, is it possible to find a region where the relative thermal unbalance may be smaller than a desired tolerance. It also can be seen that both SMAX and SSUM approach zero much sooner than the relative unbalance in heat transfer rate. This is why we chose the parameter GM as the first criterion for checking convergence. The average value of the heat transfer

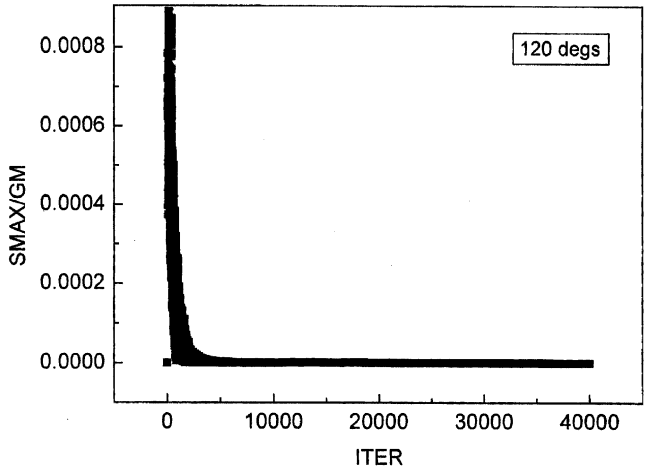

(a) $\theta = 120^\circ$

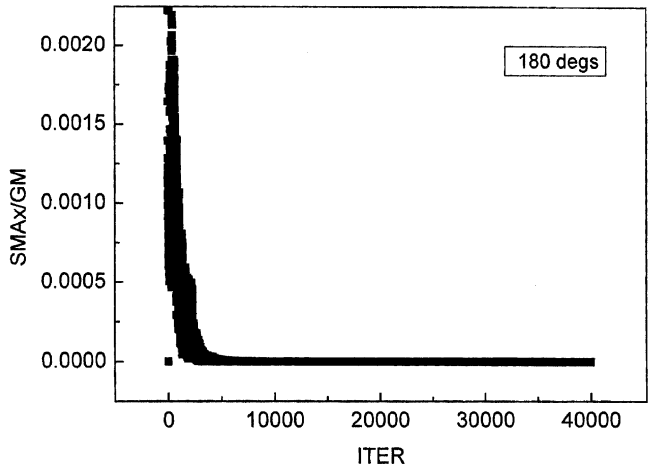

(b) $\theta = 180^\circ$

Figure 10. Variation of the relative maximum control volume mass flow residual with iteration number.

rates at the cold and hot walls are taken as the convective heat transfer loss of the envelope.

Grid-independence examination of the numerical solutions was conducted for $\theta = 110^\circ$. The average heat transfer rate was taken as the index for judging whether the grid system adopted may be considered fine enough for engineering computations. Nine grid systems were examined: $13 \times 13 \times 48$ (8,112 in total), $15 \times 15 \times 60$ (13,500 in total), $18 \times 18 \times 64$ (20,736), $19 \times 19 \times 74$ (26,714), $20 \times 20 \times 80$ (32,000), $20 \times 20 \times 90$ (36,000), $22 \times 22 \times 90$ (43,560), $22 \times 22 \times 100$ (48,400), and $22 \times 22 \times 110$ (53,200). The variation of the average heat transfer rate with

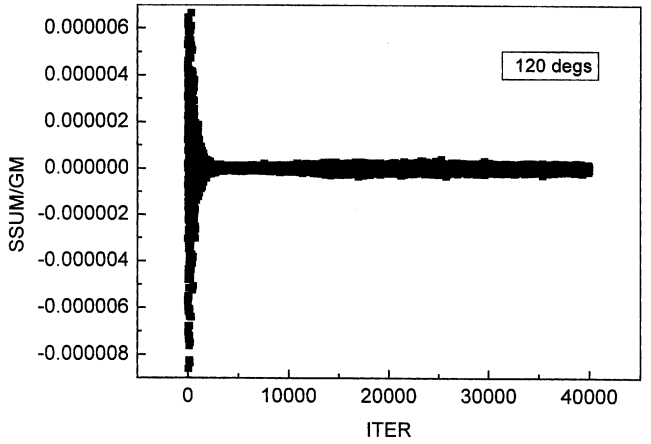

(a) $\theta = 120^{\circ}$

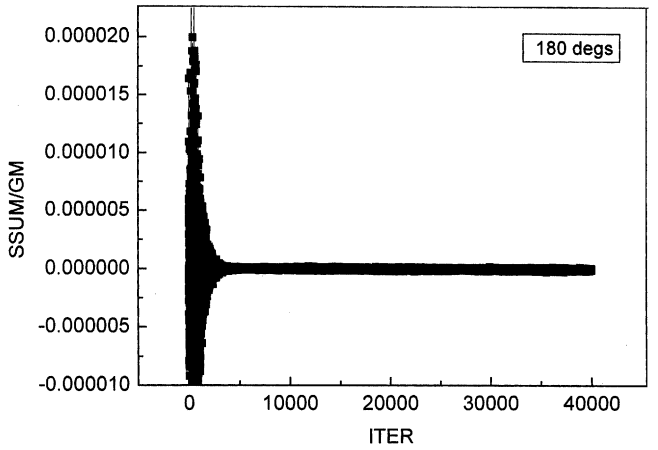

(b) $\theta = 180^{\circ}$

Figure 11. Variation of SSUM/GM with iteration number.

grid point is presented in Figure 13. As can be seen there, the numerical solution from the grid system with $20 \times 20 \times 80$ grid points can be considered as a grid-independent solution. Thus all the computations were conducted using this grid system.

Note that for a given grid system, that the value of GM approaches constant is the first criterion for checking convergence. However, for checking the grid independence of the numerical solution, this condition was not used. This is because with increase in the grid number in the z direction, the positions of cross sections at which the terms in Eq. (9) are calculated also vary. It is obvious that if a cross section is just across a center of a local vortex, the integral defined in Eq. (9) will

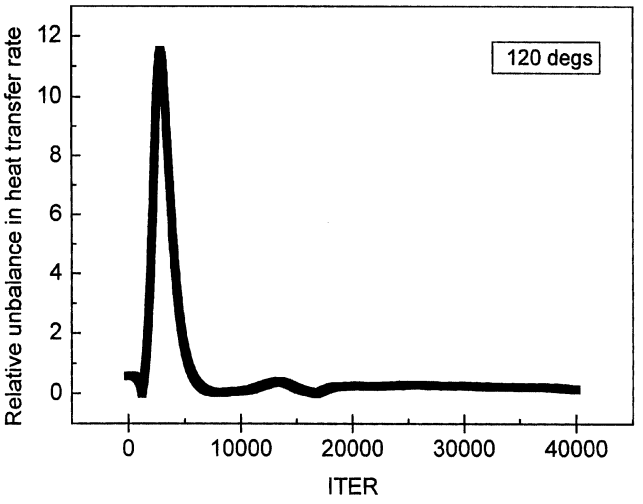

(a) $\theta = 120^\circ$

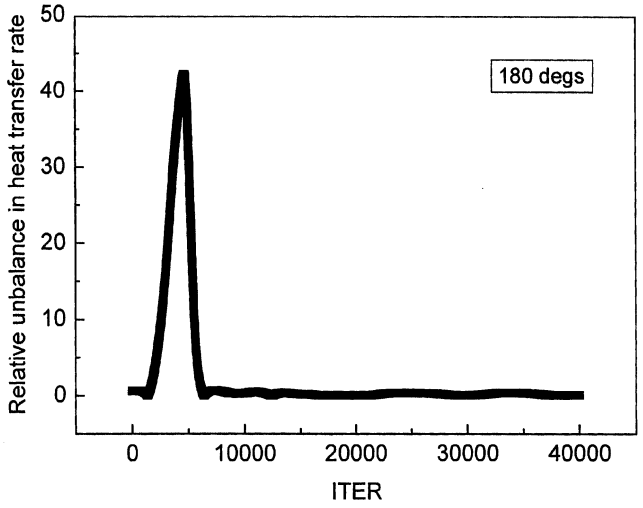

(b) $\theta = 180^\circ$

Figure 12. Variation of relative unbalance in heat transfer rates at two ends with iteration number.

be the largest. Departure from the center position of a local vortex will lead to a lower value of the integral. Thus the variation of grid number in the z direction leads to diverse numbers of the cross sections which go through the center of local vortex, and the value of the GM does not vary consistently with the increase of grid number in the z direction. Therefore the heat transfer rate was taken as the major criterion for checking the grid independency.

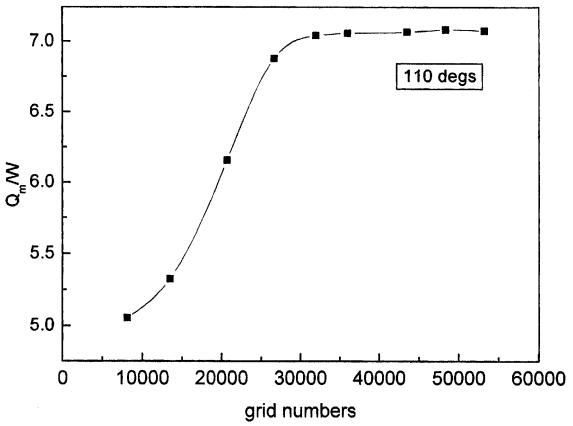

Figure 13. Grid-independence examination.

5. PRELIMINARY COMPUTATION RESULTS

The three-dimensional code was first verified by computations of several benchmark problems occurring in cylindrical coordinates, including the sudden expansion of laminar flow in a tube, natural convection in a horizontal annulus, and natural convection in a vertical annulus. All the predicted flow patterns, temperature contours, and some representative parameters agree well with the available solutions or test results in the literature [33–35]. For example, for sudden expansion in a tube, the predicted reattachment positions for $\mathrm{Re} = 50$, 100, 150, and 200 agree with the experimental results in [33] within a deviation of 2.1–5.3%. For natural convection in a horizontal annulus, the predicted equivalent thermal conductivities for $\mathrm{Ra} = 1{,}000$–5,000 agree with the test results in [34] with a range of -0.56% to 2.57%. These comparisons give strong support to verification of the developed code.

Preliminary computations were then conducted to verify the physical model and numerical treatments developed in this article. Taking the experimental results in [16] as the comparison basis, computation was conducted for the case of horizontal position with a temperature difference between the two ends of 70°C. The working fluid was helium. The predicted temperature and w-velocity component distributions along the vertical diameter of the center cross section of the envelope are presented in Figure 14. It can be seen that in the majority of the diameter the fluid temperature varies almost linearly, indicating the existence of a stratified core in the tube. The distribution of the w component shows that there are two major streams in the tube, the upper stream which is going from the hot end to the cold end, and the lower stream, going in the opposite direction. Such a flow pattern agrees qualitatively with the measured result of [16] very well, providing strong support for the numerical methods developed.

6. CONCLUSIONS

A three-dimensional steady model was established to predict the natural convection in a cylindrical envelope with fully variable thermophysical properties. The cylindrical lateral wall was assumed to be adiabatic. The two ends of the envelope

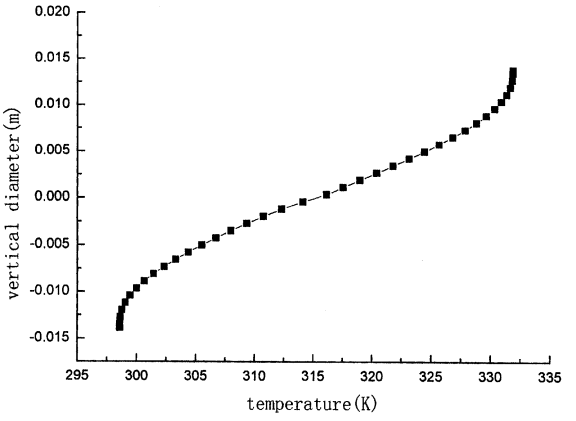

(a) Temperature

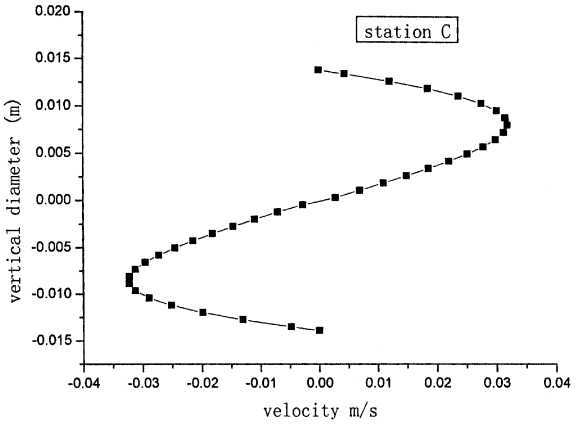

(b) Axial velocity

Figure 14. Temperature and velocity distributions along vertical diameter at cross section of $z = 0.119$ m: *(a)* temperature; *(b)* axial velocity.

were kept at constant but different temperatures. This model serves to simulate the heat transfer process in a pulse tube working at low frequency. The peculiar characters of the iterative solution procedure were revealed and a set of convergence criteria were proposed. Discussion of the rationality of adopting the power-law scheme was provided. Grid-independence examination was conducted for $\theta = 110°$, and it was found that the grid system of $20 \times 20 \times 80$ grid points with grids in the z direction being nonuniformly positioned can yield a grid-independent solution. Preliminary computation showed good qualitative agreement of the temperature and velocity distribution along the vertical diameter in the center cross section.

REFERENCES

1. T. H. Kuhen and R. J. Goldstein, An Experimental and Theoretical Study of Natural Convection in the Annulus between Horizontal Concentric Cylinders, *J. Fluid Mech.*, vol. 74, pp. 605–719, 1976.
2. M. C. Charrie-Mojtabi, A. Motabi, and J. P. Catagirone, Numerical Solution of a Flow due to Natural Convection in Horizontal Cylindrical Annulus, *ASME J. Heat Transfer*, vol. 101, pp. 171–173, 1979.
3. T. H. Kuehn and R. J. Goldstein, A Parametric Study on Prandtl Number and Diameter Ratio Effects on Natural Convection Heat Transfer in Horizontal Cylindrical Annulus, *ASME J. Heat Transfer*, vol. 102, pp. 768–770, 1980.
4. G. De Vahl Davis, Natural Convection of Air in Square Cavity, *Int. J. Numer. Meth. Fluids*, vol. 3, pp. 249–264, 1983.
5. M. Keyhani, F. A. Kulacki, and R. N. Christensen, Free Convection in a Vertical Annulus with Constant Heat Flux on the Inner Wall, *ASME J Heat Transfer*, vol. 105, pp. 454–459, 1983.
6. H. Ozoe, A. Mouri, M. Ohmoro, S. W. Churchill, and N. Lior, Numerical Calculations of Laminar and Turbulent Natural Convection in Water in Rectangular Channels Heated and Cooled Isothermally on the Opposing Vertical Walls, *Int. J. Heat Mass Transfer*, vol. 28, pp. 125–138, 1985.
7. A. W. Date, Numerical Prediction of Natural Convection Heat Transfer in Horizontal Annulus, *Int. J. Heat Mass Transfer*, vol. 29, pp. 1457–1464, 1986.
8. T. Saitoh and K. Hirose, High Accuracy Benchmark Solutions to Natural Convection in a Square Cavity, *Comput. Mech.*, vol. 4, pp. 417–427, 1989.
9. M. Hortman and M. Peric, Finite Volume Multigrid Prediction of Laminar Natural Convection: Benchmark Solutions, *Int. J. Numer. Meth. Fluids*, vol. 18, pp. 695–719, 1994.
10. G. Barakos and E. Mitsoulis, Natural Convection Flow in a Square Cavity Revisited: Laminar and Turbulent Models with Wall Function, *Int. J. Numer. Meth. Fluids*, vol. 18, pp. 695–719, 1994.
11. J. G. Wei and W. Q. Tao, Numerical Study of Natural Convection in a Vertical Annulus with Constant Heat Flux on the Inner Wall, *Int. J. Numer. Meth. Heat Fluid Flow*, vol. 6, pp. 31–46, 1996.
12. J. G. Wei and W. Q. Tao, Three-Dimensional Numerical Simulation of Natural Convection Heat Transfer in an Inclined Cylindrical Annulus, *J Thermal Sci.*, vol. 5, pp. 175–183, 1996.
13. S. W. Hong, Natural Circulation in Horizontal Pipes, *Int. J. Heat Mass Transfer*, vol. 20, pp. 685–691, 1977.
14. A. Bejan and C. L. Tien, Fully Developed Natural Counterflow in a Long Horizontal Pipe with Different End Temperatures, *Int. J. Heat Mass Transfer*, vol. 21, pp. 701–708, 1978.
15. D. D. Gray and A. Giorgin, The Validity of the Boussinesq Approximation for Liquids and Gases, *Int. J. Heat Mass Transfer*, vol. 19, pp. 545–551, 1976.
16. S. Kimura and A. Bejian A, Experimental Study of Natural Convection in a Horizontal Cylinder with Different End Temperatures, *Int. J. Heat Mass Transfer*, vol. 23, pp. 1117–1126, 1980.
17. S. H. Baek, E. S. Jeong, and S. Jeong, Two-Dimensional Model for Tapered Pulse Tubes, Part 1: Theoretical Modeling and Net Enthalpy Flow, *Cryogenics*, vol. 40, pp. 379–385, 2000.
18. G. Thummes, M. Schreiber, R. Landgraf, and C. Heiden, Convective Heat Losses in Pulse Tube Coolers: Effect of Pulse Tube Inclination, in R. G. Ross (ed.), *Cryocoolers 9*, Plenum Press, New York, 1997.
19. F. P. Incropera and D. A. Dewitt, *Introduction to Heat Transfer*, 3rd ed., pp. 478–479, Wiley, New York, 1996.

20. W. M. Kays and M. E. London, *Convective Heat Transfer and Mass Transfer*, 2nd ed., p. 315, McGraw-Hill, New York, 1980.
21. A. Lankhorst, Laminar and Turbulent Natural Convection in Cavities: Numerical Modeling and Experimental Validation, Ph.D. thesis, Delft University of Technology, Delft, The Netherlands, 1991.
22. R. F. Barron, *Cryogenic Heat Transfer*, Taylor & Francis, New York, 1999.
23. Y. L. He, Theoretical and Experimental Investigations on the Performance Improvements of Split-Stirling Refrigerator and Pulse Tube Cryocooler, Ph.D. thesis, Xi'an Jaiotong University, Xi'an, China, 2002.
24. Y. L. He, W. Q. Tao, T. S. Zhao, and Z. Q. Chen, Steady Natural Convection in a Tilted Long Cylindrical Envelope with Lateral Adiabatic Surface, Part 2: Heat Transfer Rate, Flow Patterns and Temperature Distributions, *Numer. Heat Transfer A*, pp. 399–431, 2003.
25. A. Bejan, *Heat Transfer*, pp. 336–337, Wiley, New York, 1993.
26. S. V. Patankar, *Numerical Heat Transfer and Fluid Flow*, McGraw-Hill, New York, 1980.
27. W. Q. Tao, *Numerical Heat Transfer*, 2nd ed., Xi'an Jiaotong University Press, Xi'an, China, 2001.
28. B. P. Leonard, and J. E. Drummond, Why You Should Not Use 'Hybrid', 'Power-Law' or Related Exponential Schemes for Convective Modeling—There Are Much Better Alternatives, *Int. J. Numer. Meth. Fluids*, vol. 20, pp. 421–442, 1995.
29. W. Q. Tao and E. M. Sparrow, The Transport Property and Convective Numerical Stability of the Steady-State and Convection Diffusion Finite Difference Schemes, *Numer. Heat Transfer*, vol. 11, pp. 491–497, 1987.
30. B. Yu, W. Q. Tao, D. S. Zhang, and Q. W. Wang, Discussion on Numerical Stability and Boundedness of Convective Discretization Scheme, *Numer. Heat transfer B*, vol. 40, pp. 343–364, 2001.
31. M. Yang and W. Q. Tao, Numerical Study of Natural Convection Heat Transfer in a Cylindrical Envelope with Internal Concentric Slotted Hollow Cylinder, *Numer. Heat Transfer A*, vol. 22, pp. 289–307, 1992.
32. P. M. Gresho, Is the Steady Viscous Incompressible Two-Dimensional Flow over a Backward-Facing Step at Re = 800 Stable?, *Int. J. Numer. Meth. Fluids*, vol. 17, pp. 501–541, 1993.
33. E. O. Macagno and T. K. Hung, Computational and Experimental Study of a Captive Annular Eddy, *J. Fluid Mech.*, vol. 28, pp. 43–61, 1968.
34. T. H. Kuehn and R. J. Goldstein, An Experimental and Theoretical Study of Annular Natural Convection in the Annulus between Horizontal Concentric Cylinders, *J. Fluid Mech.*, vol. 74, pp. 605–719, 1976.
35. J. G. Wei and W. Q. Tao, A Numerical Study of Natural Convection in a Vertical Annulus with Constant Heat Flux on the Inner Wall, *Int. J. Numer. Meth. Heat Fluid Flow*, vol. 6, pp. 31–46, 1996.